## PAPER

Check for updates

# Chemical gradients on graphene *via* direct mechanochemical cleavage of atoms from chemically functionalized graphene surfaces†

Hyeonsu Kim,[a] Dong-Hyun Kim, [ID][bc] Yunjo Jeong,[b] Dong-Su Lee,[b] Jangyup Son*[bd] and Sangmin An [ID] *[a]

Manipulating the surface chemistry of graphene is critical to many applications that are achievable by chemical functionalization. Specifically, tailoring the spatial distribution of functional groups offers more opportunities to explore functionality using continuous changes in surface energy. To this end, careful consideration is required to demonstrate the chemical gradient on graphene surfaces, and it is necessary to develop a technique to pattern the spatial distribution of functional groups. Here, we demonstrate the tailoring of a chemical gradient through direct mechanochemical cleavage of atoms from chemically functionalized graphene surfaces *via* an atomic force microscope. Additionally, we define the surface characteristics of the fabricated sample by using lateral force microscopy revealing the materials' intrinsic properties at the nanoscale. Furthermore, we perform the cleaning process of the obtained lateral force images by using a machine learning method of truncated singular value decomposition. This work provides a useful technique for many applications utilizing continuous changes in the surface energy of graphene.

## 1. Introduction

Graphene has garnered significant attention due to its unique and extraordinary electronic, mechanical, and chemical properties since it was successfully exfoliated from graphite by a peeling method called micromechanical cleavage.[1] Thereafter, remarkable progress in large-area growth techniques of graphene has made possible a variety of its applications including in transparent, stretchable, and wearable electronics.[2–5] However, it has been challenging to expand applications due to certain limitations, such as a zero band gap, inert surface chemistry, and weak electrochemical activity.[6,7] In this regard, there have been extensive studies on the surface modification of graphene *via* chemical functionalization to open its band gap[8–10] or to tune its surface energy.[11] Especially, the chemical modification of graphene surfaces has relied mostly on plasma treatment,[12–14] which allowed for the modification of graphene's characteristics such as surface friction and band gap.[15]

Consequently, it pioneered a new era of application of graphene such as gas sensors,[16] high-performance dielectric materials[17] and microscale solid lubricants.[18]

While the strategy of attaching atoms or functional groups for surface control of two-dimensional (2D) materials has been widely studied,[19,20] controlling the surface of 2D materials by removing such atoms or functional groups is also being highlighted,[21] especially the surface modification of the chemical gradient.[22] The chemical gradient is a linear gradient in the form of a slope created by artificially manipulating the density of functionalized groups (O and F) in a functionalized graphene area. The region where physical properties change on one material has a region where a semiconductor changes to a conductor due to graphene with conductor properties and functionalized graphene with semiconductor properties.[23] At the same time, it has a very unique property that hydroiodic graphene and hydrophilic functionalized graphene change linearly.[15] There are limitations in conventional plasma processing methods or masking methods to pattern the spatial distribution at the nanoscale. However, it is possible to tailor an elaborate chemical gradient by scrubbing the surface of 2D materials with a sharp atomic force microscope (AFM) tip. Contact-mode AFM is a technology that can directly interact with samples and obtain physical properties of the surface based on a very small force (typically 10–50 nN) in the repulsive region of the Lennard-Jones potential generated between the sharp tip of the AFM and the sample. Because direct interaction between the AFM tip and the sample may cause damage to both

[a]*Department of Physics, Institute of Photonics and Information Technology, Jeonbuk National University, Jeonju 54896, South Korea. E-mail: san@jbnu.ac.kr*

[b]*Functional Composite Materials Research Center, Korea Institute of Science and Technology, Jeonbuk 55324, South Korea. E-mail: jayson@kist.re.kr*

[c]*SKKU Advanced Institute of Nanotechnology (SAINT), Sungkyunkwan University, Suwon 16419, South Korea*

[d]*Division of Nano and Information Technology, KIST School University of Science and Technology (UST), Jeonbuk 55324, South Korea*

† Electronic supplementary information (ESI) available. See DOI: https://doi.org/10.1039/d3na00066d

the tip and sample surface due to generation of high pressure exerted by the tip on the sample, it can be also used to obtain data on surface friction,[24] and one can investigate the naturally confined water meniscus between the sharp tip and the sample affecting the friction behavior,[25] In addition, contact-mode AFM can be used not only for characterizing the sample surface, but also for the nanomanipulation of particles on the sample at the atomic level.[26] Moreover, it can be used to modify the bond between graphene and the substrate and ultimately the surface electrical properties of graphene by using the high pressure of diamond tips.[27]

Recently, Felts *et al.* introduced a method of direct mechanochemical cleavage of functional groups on chemically modified graphene (CMG) by using contact-mode AFM,[21] demonstrating that the mechanochemical reaction rate is determined by chemical properties of the AFM tip, the force between the tip and the sample, and the dwell time – determined by another scan parameter such as the contact radius and tip speed. However, there have been no systematic studies on elaborate techniques to pattern continuous chemical gradients on 2D surfaces, despite their potential applications in basic and applied studies utilizing changes in the gradient surface energy landscape (*e.g.*, voluntary movement of water droplets, application of electronic elements due to continuous changes in the bandgap, applications using thermal conductivity changes, differences in atomic deposition due to surface energy differences, *etc.*). Here, we further demonstrate a chemical gradient *via* mechanochemical cleavage of adatoms on the CMG (fluorinated or hydrogenated graphene) by *in situ* adjustment of the mechanochemical reaction during standard contact-mode AFM, achieved through a change in both the normal load and dwell time in the slow scan direction and tip speed in the fast scan direction (Fig. S1†). We evaluated the surface characteristics of CMG with lateral force microscopy (LFM) that indicates friction information of the surface of the sample by using the fact that the CMG has higher friction than pristine graphene.[15] Furthermore, we demonstrate an effective image processing technique for optimizing the obtained LFM images using the truncated singular value decomposition method (SVD) to eliminate noise from data.[28,29]

## 2. Experimental details

### 2.1. Fluorination and hydrogenation of graphene

We prepared a large-area monolayer graphene film on copper foil by the chemical vapor deposition method.[30,31] Graphene was chemically functionalized by either $CF_4$ plasma ($CF_4$ 20 sccm, 150 W, 50 mTorr, and 1 min) for fluorination or $H_2$ plasma ($H_2$ 40 sccm, 50 W, 10 mTorr, and 10 min) for hydrogenation. We confirmed the chemical specifications of the fabricated fluorinated graphene and hydrogenated graphene comparing with pristine graphene by using Raman spectra (Fig. S2†). As shown in Fig. S3,† the exfoliated monolayer pristine graphene was treated *via* $CF_4$ plasma, and the Raman mapping image shows a uniform D-peak intensity, which indicates that the graphene surface was uniformly changed to a fluorinated surface. Although non-uniform D-peak intensity was confirmed at the

edges of graphene, the central area of fluorinated graphene (FG) in which the mechanical defluorination experiment is performed with the AFM tip is a uniformly fluorinated area.

### 2.2. Mechanochemical cleavage by using AFM

We performed gradient mechanochemical cleavage of the fluorinated or hydrogenated graphene by using a conventional AFM (NX10, Park System Co.) with a contact-mode silicon cantilever (PPP-CONSTSCR, NANOSENSORS™) which has a force constant of about 0.2 N m$^{-1}$ and a resonance frequency of about 23 kHz under ambient conditions (Table S1†). According to a previous study,[21] for the mechanochemical reaction rate determined by using the normal load, dwell time and chemical properties of the AFM tip, we create a potential gradient on CMG with a combination of adjusting the normal load for step variation of the slow scan direction (Fig. S4†) and dwell time, which are important factors to adjust properly and continuously to determine the mechanochemical reaction rate. In other to control the dwell time, we fixed the line space for the slow scan direction typically in 32 steps, by adjusting the normal load and controlled speed of the tip during scanning. Note that we assume the wear of the tip radius due to damage during scanning,[21] which is another factor that determines the dwell time, is small. Damage to the tip is unavoidable. However, the area where the potential gradient was created in this work is a small area of several μm$^2$. It is reported that the scission of chemical bonding due to contact is inversely proportional to the 4th power of the contact radius of the tip, so if the damage of the tip is assumed to be large, uniform surface friction in the area pressed with the same force and increasing surface friction in the slow scan direction should be obtained; however, we could not find such results. And it is difficult to check the graphene damage with height information when there are contaminants on the surface, since the graphene on the SiO$_2$ substrate has a height of about 3 Å. However, graphene, CMG, and SiO$_2$ have different surface friction characteristics, and thus, if graphene is damaged, it can be easily identified through LFM data. However, considerably high pressure is required to damage graphene in contact mode AFM such as graphene damage at a high force of ∼950 nN using a diamond coated cantilever and changing the electrical properties of bi or multilayer graphene using a diamond cantilever.[26] We could not find such graphene damage.

## 3. Results and discussion

### 3.1. Potential gradient mechanochemical cleavage on exfoliated & fluorinated graphene

Fig. 1 shows the schematic illustration describing our technique to pattern the chemical gradient on the graphene surface *via* mechanochemical cleavage of adatoms from the chemically modified graphene. We controlled the reaction rate by precisely adjusting the factors (dwell time and normal load) to create a potential gradient by intentionally grading the density of functional groups on the surface. The cleavage degree of the functional group when the tip physically comes into contact with the sample shows an exponential decay characteristic of the
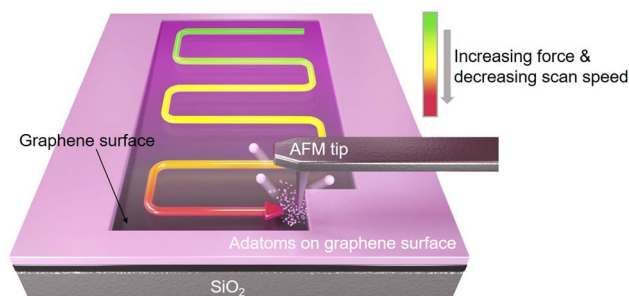
**Fig. 1** Fabrication schematic of gradient mechanochemical cleavage of the fluorinated or hydrogenated graphene *via* a contact-mode cantilever of an atomic force microscope.

energy activation barrier by the product of the applied stress and the activation volume, and is affected by temperature.[21] Therefore, when performing an experiment at a fixed temperature, if the product of the stress applied to the sample by the tip and the activation volume is sufficiently greater than the energy activation barrier of the sample, the functional group can be separated by the tip. The degree of breakage of the bond between the functional group and graphene is affected by several scan parameters, such as the pressing force, the distance between scan lines, the speed of the tip, and the contact area between the

tip and the sample. Therefore, in order to create a gradient on functionalized graphene, the above parameters are continuously changed so that the scan can be performed with a feasible scan speed and normal force while reducing the time required for scanning, and thereby, adjusting the density of the functional group to create a gradient on the surface was performed.

Fig. 2a and b show the topography and LFM images of exfoliated & fluorinated graphene. Gradient mechanochemical cleavage of the fluorinated graphene was performed to produce a $1 \times 1$ μm gradient by gradually removing the attached fluorine atoms. 2048 lines were scanned to allow the line space in the slow scan direction to be 0.48 nm with a resulting scan range of ~1 μm, and the normal load variation range was set from 20 nN to 105 nN (32 steps in the slow scan direction) along with a corresponding tip speed range of 50 Hz–0.5 Hz (line scan rate) under a condition of linear control. After this, we confirmed the result of the gradient mechanochemical cleavage with an additional wider LFM scan ($1.3 \times 1.3$ μm) along with a low set point of normal load (5 nN) and fast tip speed (10 Hz) for evaluation (low dwell time prevents undesired removal of the chemical groups). Fig. 2d shows the LFM image indicating frictional information corresponding to the height information (Fig. 2c), which confirms that the functional groups of fluorinated graphene are successfully cleaved gradually in the desired pattern. The surface contaminants shown as white spots in Fig. 2 had an average height of
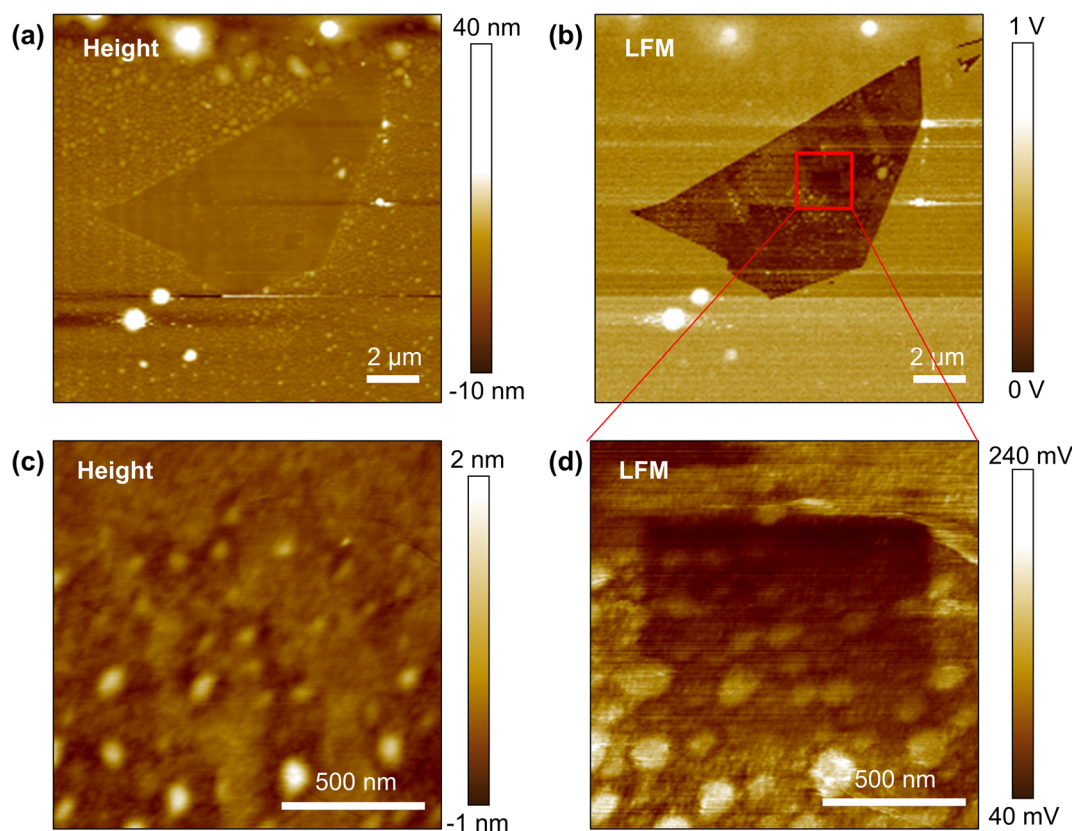


**Fig. 2** Gradient mechanochemical cleavage of the fluorinated graphene by using a contact-mode AFM by controlling the normal load (20 nN– 105 nN) and the tip speed (scan rate of 50 Hz–0.5 Hz) with a step interval of 32. (a and b) Height and LFM images of the fluorinated graphene flake on SiO$_2$. (c and d) Magnified height and LFM images of the gradient mechanochemical cleavage of the fluorinated graphene.

approximately 3 nm and did not interfere with the tip–surface interaction or the quality of the fabricated chemical gradient.

### 3.2. Potential gradient mechanochemical cleavage on the CVD & hydrogenated graphene

Next, we demonstrated the gradient mechanochemical cleavage of hydrogen atoms attached to the surface of graphene prepared *via* CVD, which is more ideal for large-scale applications (Fig. 3). We performed the production of gradient mechanochemical cleavage on $3 \times 3$ μm of hydrogenated CVD graphene. 3072 lines were scanned to allow the line space between slow scans to be 0.97 nm, and the normal load (20 nN–120 nN)/and speed of the tip (line scan rate of 50 Hz–0.5 Hz) were both linearly controlled. An additional scan was performed for evaluation ($4.2 \times 4.2$ μm). Fig. 3a shows the average height line profile of the slow scan direction from the scanned height image (white dashed box) of the gradient mechanochemical cleavage on hydrogenated CVD graphene (Fig. 3b), and we point out the flatness of the height profile in the inset of the graph. Fig. 3c shows the average LFM signal line profile of the slow scan direction from the scanned LFM image (white dashed box) of the gradient mechanochemical cleavage on hydrogenated CVD

graphene (Fig. 3d), and we point out the gradient profile from the LFM data in the inset of the graph. Note that surface cleanliness is a crucial factor in performing precise gradient mechanochemical cleavage. We find that if there are large contaminants on the surface of the graphene, it is difficult to define the formation of ramping (normal load & dwell time) due to the interference between the tip and the contaminated surface (Fig. 3b). We note that one can perform this experiment with other combinations such as CVD & fluorinated graphene and exfoliated & hydrogenated graphene.

### 3.3. Potential gradient mechanochemical cleavage of the wide area (CVD & hydrogenated graphene)

Typically, one can fabricate a relatively wide area of the graphene sheet by using the CVD method instead of the exfoliation method. Thus, we demonstrated the gradient mechanochemical cleavage of the hydrogen atom attached CVD graphene by verifying the fabrication capability of a wide surface area compared to that of the mechanically exfoliated graphene (Fig. 4). We demonstrate the potential gradient of $10 \times 10$ μm on hydrogenated graphene, and a total of 10 240 lines was scanned to allow the line space between slow scans to be
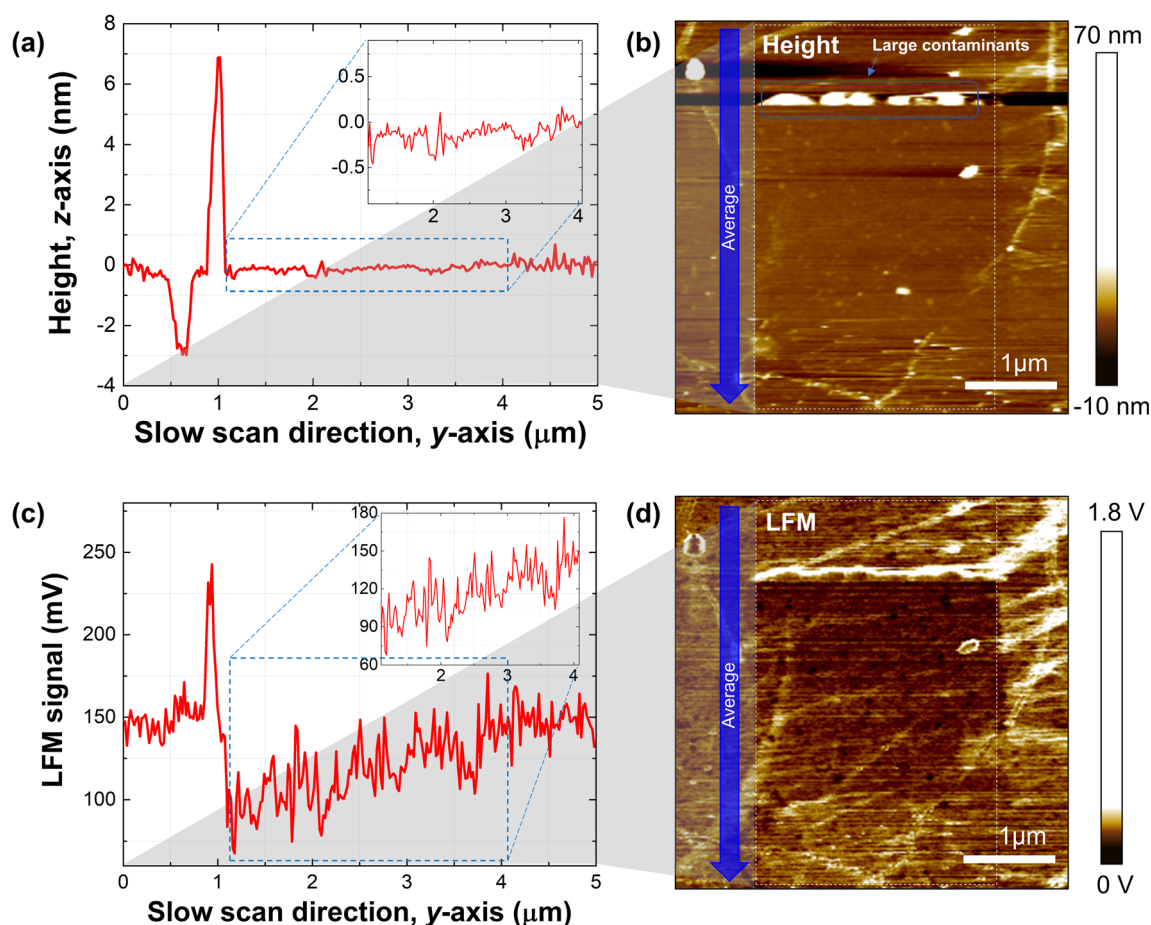


**Fig. 3** Gradient mechanochemical cleavage of the CVD and hydrogenated graphene under a condition of the normal load (0–120 nN) and the tip speed (line scan rate of 50–0.5 Hz) with a step interval of 32. (a) Average height profile data extracted vertically. (b) Height image showing mechanochemical cleavage on surface of hydrogenated graphene. (c) Average LFM signal profile data extracted vertically. (d) Lateral image showing mechanochemical cleavage on surface of hydrogenated graphene.
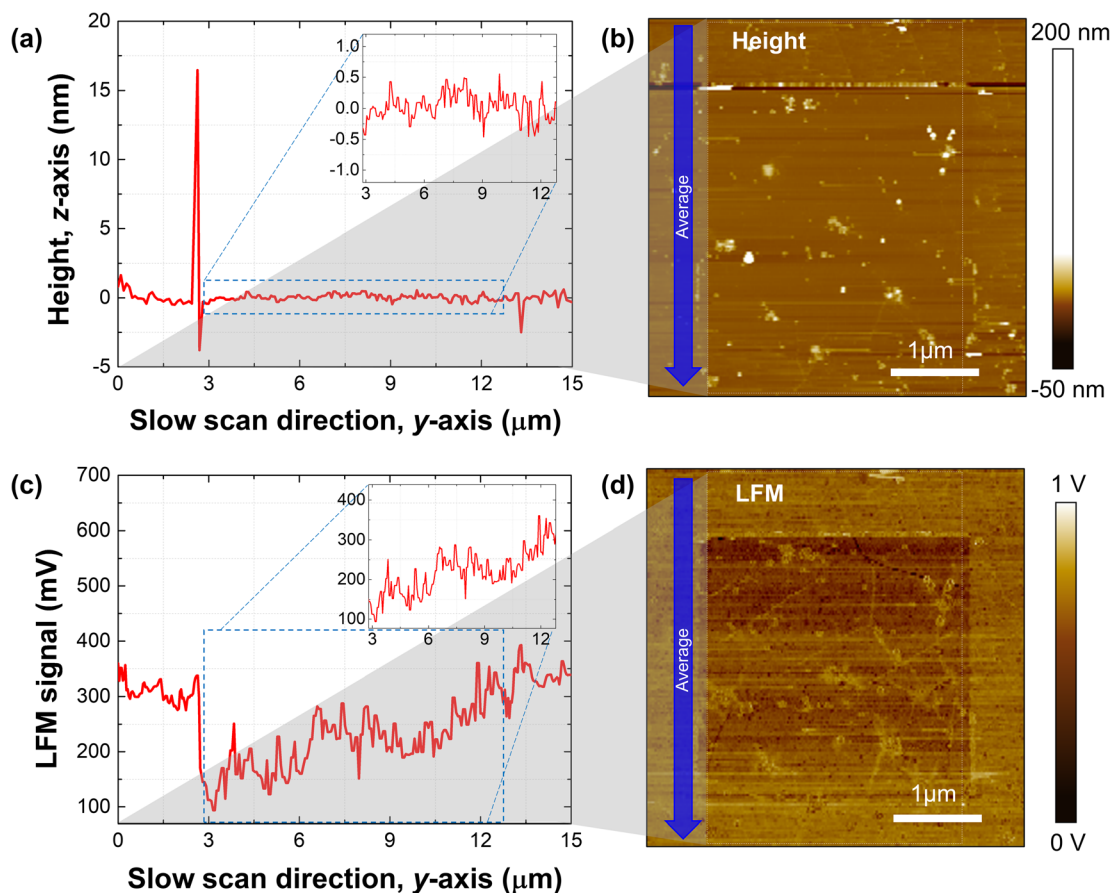
**Fig. 4** Gradient mechanochemical cleavage of the wide area (10 × 10 μm, CVD & hydrogenated graphene) under a condition of the normal load (10–103 nN) and the tip speed (line scan rate of 10–0.18 Hz) with a step interval of 32. (a) Average height profile data extracted vertically, (b) height image showing mechanochemical cleavage on surface of CVD & hydrogenated graphene. (c) Average LFM signal profile data extracted vertically (d) lateral image showing mechanochemical cleavage on surface of CVD & hydrogenated graphene.

0.97 nm, and the normal load (10 nN–103 nN)/and speed of the tip (line scan rate of 10 Hz–0.18 Hz) were all linearly controlled. Fig. 4a shows the average height line profile of the slow scan direction from the scanned height image (white dashed box) of the wide range gradient mechanochemical cleavage in a wide range of hydrogenated CVD graphene (Fig. 4b), confirming the flatness of the height profile in the inset of the graph, while Fig. 4c shows the average LFM signal line profile of the slow scan direction from the scanned LFM image (white dashed box) of the gradient mechanochemical cleavage on hydrogenated CVD graphene (Fig. 4d), confirming the gradient profile from the LFM data in the inset of the graph. Note that the created ramp area (10 × 10 μm) is relatively large, which indicates that the total traveling distance of the tip is long enough; thus, one can assume that the contact radius of the tip increases by tip wear resulting in an increment of the dwell time gradually differing from the beginning to the end during scanning. However, we found that the tip radius variation by a relatively long-time scan shows no big issue for the results, and rather, the normal load and tip speed are more dominant factors for the performance of the gradient mechanochemical cleavage. More interestingly, at the wide surface area, grain boundaries (GBs) are observed (see the lines in Fig. 4d). Normally, the

binding energy of adatoms with carbon atoms at the GB is stronger than that of adatoms and carbon atoms on the basal plane; therefore, we assume that adatoms on GBs are not eliminated *via* mechanochemical cleavage.[32,33] Moreover, we consider this observation positive since our technique provides an opportunity to pattern adatoms only on the GBs on the graphene surface. The bond between adatoms and graphene has stronger binding energy at GBs and in the winkle region than in flat regions.[33] Therefore, separation of H or F in graphene GBs and the winkle region requires a higher pressure than the pressure required for separation in a flat area, so selective removal might be possible at the GB and in the winkle region. And this can explain why the functional groups in GBs and the winkle region in Fig. 3 and 4 are still intact.

### 3.4. Data optimization of the lateral force images *via* singular value decomposition (SVD)

The data obtained from the aforementioned experiments inevitably display undesired noise, caused by various environmental factors. Although it is possible to minimize these things in the sample fabrication process,[34,35] it is virtually impossible to eliminate all causes of noise. And these contaminants not only
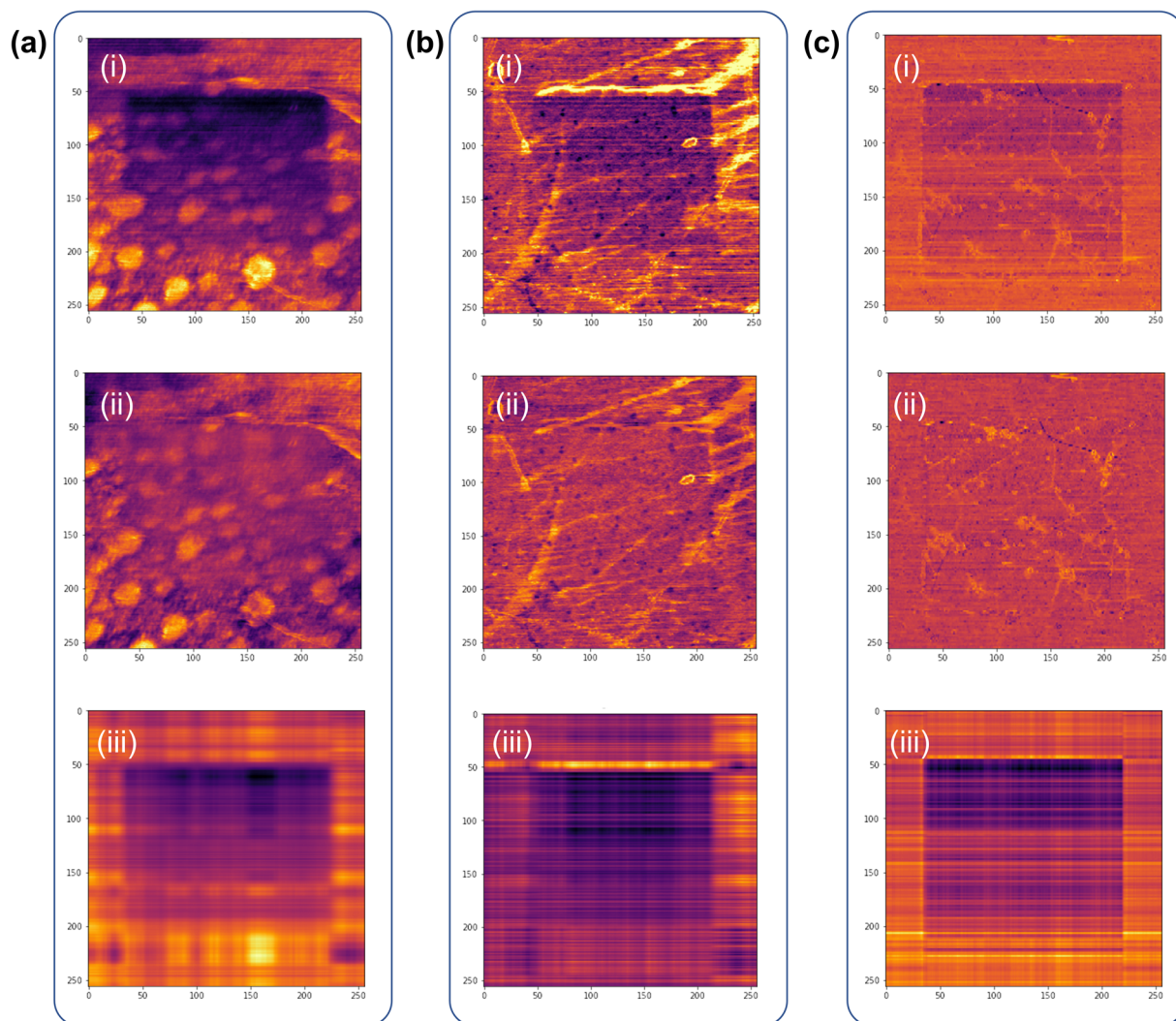
**Fig. 5** Data cleaning process (pixels). (a) Gradient mechanochemical cleavage on the exfoliated & fluorinated graphene of 1 × 1 μm ((i) original data, (ii) removed data, and (iii) cleaned data). (b) Gradient mechanochemical cleavage on the CVD & hydrogenated graphene of 3 × 3 μm ((i) original data, (ii) removed data, and (iii) cleaned data). (c) Gradient mechanochemical cleavage on the wide area (10 × 10 μm) of CVD & hydrogenated graphene ((i) original data, (ii) removed data, and (iii) cleaned data).

hinder proper contact between the AFM tip and the graphene surface, but also inhibit optimal evaluation of the gradient mechanochemical cleavage data obtained from LFM. Thus, we employed a machine-learning based linear algebraic approach of truncated singular value decomposition (SVD) to extrapolate relevant experimental data from the raw data, as shown in Fig. 5.[36] SVD is a linear algebra operation used for separating matrices in descending order; truncated SVD operates by reconstructing these separated matrices and removing irrelevant data from the raw data by manually selecting the principal components of the diagonal matrices (ESI note, Fig. S5†). The data optimization processes for the raw gradient mechanochemical cleavage data of 1 × 1 μm, 3 × 3 μm, and 10 × 10 μm are shown in Fig. 5. In addition, Fig. S6† shows the 3D profiles of the 1 × 1 μm and 10 × 10 μm results.

Fig. 6 shows that the average value of the separated data is maintained and there is almost no data deformation caused by the truncated SVD cleaning process. As the standard deviation is reduced, we evaluate the results of gradient mechanochemical cleavage clearly by removing unnecessary data and distinguish each data cluster in the histogram. Therefore, this indicates that truncated SVD can be used to increase the performance of the clustering algorithm. Fig. 6a(i), b(i) and c(i) show the mean values of the line profile of the LFM images (1 × 1 μm, 3 × 3 μm, and 10 × 10 μm) comparing the original raw data of gradient mechanochemical cleavage (black line) to the cleaned data (red line), demonstrating that truncated SVD does not affect the average value of the data. In addition, because the LFM data are considered as a combination of scratched CMG and bare CMG showing two different values of the friction signal, one can expect that there are two shapes of the histogram peak. Thus, it is difficult to distinguish these two peaks in noisy raw data (black dots of Fig. 6a(ii), b(ii) and c(ii)). However, we clearly observed two different peaks in the data cleaned by usage of the truncated SVD method (red dots of Fig. 6a(ii), b(ii) and c(ii)).
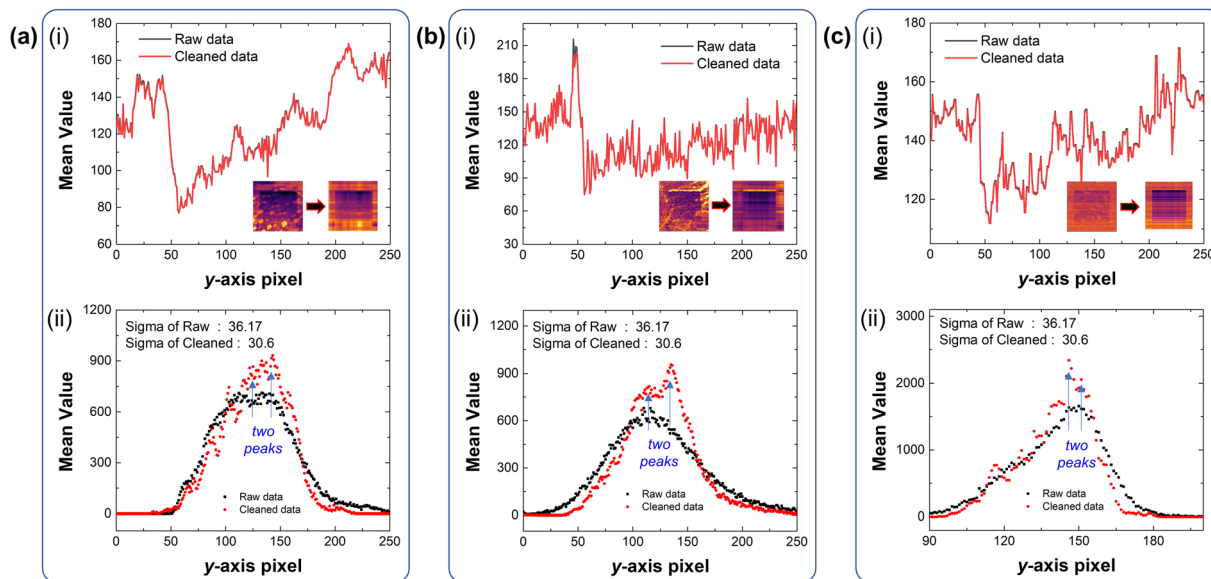
Fig. 6 Confirmation of the mean values of the separated data without data deformation by using the truncated SVD cleaning process on the gradient mechanochemical cleavage data of (a) $1 \times 1$ μm, (b) $3 \times 3$ μm, and (c) $10 \times 10$ μm.

### 3.5. Chemical gradient for future applications (discussion)

The advantages of gradient patterning using AFM are as follows. (i) Unlike the previous method of creating a gradient by adjusting the reach of plasma using an additional mask during plasma processing,[22] a gradient can be created even in a small area without a mask requiring additional processing. (ii) Patterning can be performed immediately at the desired location. (iii) Using the fact that the surface friction of graphene and functionalized graphene is different immediately after patterning, the gradient on the surface can be immediately checked through LFM, and parameter optimization can be quickly performed to create the desired gradient.

An important difference from ref. 21 is that the form of erasing fluorene can be created as a gradient. This can be seen as a preparation step for an important application from an energy point of view. If a surface with a difference in gradient surface potential is placed in an ionic liquid such as an electrolyte, the ions move to one side due to the difference in surface potential and generate an electric current. Therefore, it is considered as a self-powered source by spontaneous current formation. Using this, $H_2O$ in moisture is combined with the chemical gradient graphene surface to generate proton-like ions, and it can be used for 'moisture electricity generation (MEG)' in which the voltage is generated by the difference in proton density.

For use as a power source by using the difference in potential of the gradient surface, it is necessary to manufacture it in a large area with AFM technology by stitching the area. In the case of patterning a large area, it inevitably meets the possibility of working on an unclean surface. This experiment was performed as a viewpoint of verification of manufacturing a chemical gradient under any condition of the surface, and it was confirmed that a clear gradient was produced through somewhat messy results or analysis techniques.

In addition, depending on the surface chemistry of functionalized graphene, the formation of a chemical gradient in which metal is deposited and grown differs, and the electrical/optical characteristics of a transition metal dichalcogenide (TMDC) appear different when bonded with a semiconducting 2-dimensional TMDC. In addition, it can be used for microfluidic research on gradient-driven liquid movement under no power circumstance through positional control of wettability based on the surface chemical gradient.

## 4. Conclusions

In this study, we demonstrated the feasibility of gradient mechanochemical cleavage in large-area fluorinated or hydrogenated graphene using a method of continuously changing the mechanochemical reaction rate by adjusting the normal load and dwell time during scanning via a contact-mode AFM. We evaluated the produced mechanochemical cleavage by LFM, confirming successful gradient formation on the CMG surface. In addition, we accurately defined the potential gradient mechanochemical cleavage by removing unnecessary information on the obtained AFM/LFM data using a truncated SVD method. This work provides a useful technique for many applications utilizing continuous changes in the surface energy of graphene, such as self-powered systems, spontaneous movement of water droplets, electronic devices utilizing continuous changes in the band gap, thermos-electronics using thermal conductivity changes, and selective atomic deposition due to surface energy differences.

## Author contributions

Hyeonsu Kim: conceptualization, methodology, investigation, writing – original draft. Dong-Hyun Kim: methodology,

## Conflicts of interest

The authors declare no conflict of interest.

## Acknowledgements

## References

1 K. S. Novoselov, A. K. Geim, S. V. Morozov, D. Jiang, Y. Zhang, S. V. Dubonos, I. V. Grigorieva and A. A. Firsov, Electric Field Effect in Atomically Thin Carbon Films, *Science*, 2004, **306**, 666–669, https://www.science.org/doi/10.1126/science.1102896.

2 K. S. Kim, Y. Zhao, H. Jang, S. Y. Lee, J. M. Kim, K. S. Kim, J.-H. Ahn, P. Kim, J.-Y. Choi and B. H. Hong, Large-scale pattern growth of graphene films for stretchable transparent electrodes, *Nature*, 2009, **457**, 706–710, DOI: **10.1038/nature07719**.

3 X. Li, W. Cai, J. An, S. Kim, J. Nah, D. Yang, R. Piner, A. Velamakanni, I. Jung, E. Tutuc, S. K. Banerjee, L. Colombo and R. S. Ruoff, Large-Area Synthesis of High-Quality and Uniform Graphene Films on Copper Foils, *Science*, 2009, **324**, 1312–1314, https://www.science.org/doi/10.1126/science.1171245.

4 S. Bae, H. Kim, Y. Lee, X. Xu, J.-S. Park, Y. Zheng, J. Balakrishnan, T. Lei, H. R. Kim, Y. I. Song, Y.-J. Kim, K. S. Kim, B. Özyilmaz, J.-H. Ahn, B. H. Hong and S. Iijima, Roll-to-roll production of 30-inch graphene films for transparent electrodes, *Nat. Nanotechnol.*, 2010, **5**, 574–578, DOI: **10.1038/nnano.2010.132**.

5 Y. Zhang, L. Zhang and C. Zhou, Review of Chemical Vapor Deposition of Graphene and Related Applications, *Acc. Chem. Res.*, 2013, **46**, 2329–2339, DOI: **10.1021/ar300203n**.

6 M. J. Allen, V. C. Tung and R. B. Kaner, Honeycomb Carbon: A Review of Graphene, *Chem. Rev.*, 2010, **110**, 132–145, DOI: **10.1021/cr900070d**.

7 L. Yan, Y. B. Zheng, F. Zhao, S. Li, X. Gao, B. Xu, P. S. Weiss and Y. Zhao, Chemistry and physics of a single atomic layer: strategies and challenges for functionalization of graphene and graphene-based materials, *Chem. Soc. Rev.*, 2012, **41**, 97–114, DOI: **10.1039/c1cs15193b**.

8 S. Gaddam, C. Bjelkevig, S. Ge, K. Fukutani, P. A. Dowben and J. A. Kelber, Direct graphene growth on MgO: origin of the band gap, *J. Phys.: Condens. Matter*, 2011, **23**, 072204, DOI: **10.1088/0953-8984/23/7/072204**.

9 G. Giovannetti, P. A. Khomyakov, G. Brocks, P. J. Kelly and J. van den Brink, Substrate-induced band gap in graphene on hexagonal boron nitride: Ab initio density functional calculations, *Phys. Rev. B: Condens. Matter Mater. Phys.*, 2007, **76**, 073103, DOI: **10.1103/PhysRevB.76.073103**.

10 S. Y. Zhou, G.-H. Gweon, A. V. Fedorov, P. N First, W. A. de Heer, D.-H. Lee, F. Guinea, A. H. Castro Neto and A. Lanzara, Substrate-induced bandgap opening in epitaxial graphene, *Nat. Mater.*, 2007, **6**, 770–775, DOI: **10.1038/nmat2003**.

11 R. Roldán, Includes a collection of articles on the theme of Graphene Chemistry, *Chem. Soc. Rev.*, 2017, **46**, 4377–4810, DOI: **10.1039/C7CS90073B**.

12 K.-J. Jeon, Z. Lee, E. Pollak, L. Moreschini, A. Bostwick, C.-M. Park, R. Mendelsberg, V. Radmilovic, R. Kostecki, T. J. Richardson and E. Rotenberg, Fluorographene: A Wide Bandgap Semiconductor with Ultraviolet Luminescence, *ACS Nano*, 2011, **5**(2), 1042–1046, DOI: **10.1021/nn1025274**.

13 I. Jung, D. A. Field, N. J. Clark, Y. Zhu, D. Yang, R. D. Piner, S. Stankovich, D. A. Dikin, H. Geisler, C. A. Ventrice Jr and R. S. Ruoff, Reduction Kinetics of Graphene Oxide Determined by Electrical Transport Measurements and Temperature Programmed Desorption, *J. Phys. Chem. C*, 2009, **113**(43), 18480–18486, DOI: **10.1021/jp904396j**.

14 R. Balog, B. Jørgensen, L. Nilsson, M. Andersen, E. Rienks, M. Bianchi, M. Fanetti, E. Lægsgaard, A. Baraldi, S. Lizzit, Z. Sljivancanin, F. Besenbacher, B. Hammer, T. G. Pedersen, P. Hofmann and L. Hornekær, Bandgap opening in graphene induced by patterned hydrogen adsorption, *Nat. Mater.*, 2010, **9**, 315–319, DOI: **10.1038/nmat2710**.

15 S. Kwon, J.-H. Ko, K.-J. Jeon, Y.-H. Kim and J. Y. Park, Enhanced nanoscale friction on fluorinated graphene, *Nano Lett.*, 2012, **12**(12), 6043–6048, DOI: **10.1021/nl204019k**.

16 K. K. Tadi, S. Pal and T. N. Narayanan, Fluorographene based Ultrasensitive Ammonia Sensor, *Sci. Rep.*, 2016, **6**, 25221, DOI: **10.1038/srep25221**.

17 K. I Ho, C.-H. Huang, J.-H. Liao, W. Zhang, L.-J. Li, C.-S. Lai and C.-Y. Su, Fluorinated Graphene as High Performance Dielectric Materials and the Applications for Graphene Nanoelectronics, *Sci. Rep.*, 2014, **4**, 5893, DOI: **10.1038/srep05893**.

18  Y. Liu, J. Li, X. Chen and J. Luo, Fluorinated Graphene: A Promising Macroscale Solid Lubricant under Various Environments, *ACS Appl. Mater. Interfaces*, 2019, **11**(43), 40470–40480, DOI: **10.1021/acsami.9b13060**.

19  D. R. Dreyer, S. Park, C. W. Bielawski and R. S. Ruoff, The chemistry of graphene oxide, *Chem. Soc. Rev.*, 2010, **39**, 228–240, DOI: **10.1039/B917103G**.

20  V. Georgakilas, M. Otyepka, A. B. Bourlinos, V. Chandra, N. Kim, K. C. Kemp, P. Hobza, R. Zboril and K. S. Kim, *Chem. Rev.*, 2012, **112**, 6156–6214, DOI: **10.1021/cr3000412**.

21  J. R. Felts, A. J. Oyer, S. C. Hernández, K. E. Whitener Jr, J. T. Robinson, S. G. Walton and P. E. Sheehan, Direct mechanochemical cleavage of functional groups from graphene, *Nat. Commun.*, 2015, **6**, 6467, DOI: **10.1038/ncomms7467**.

22  S. C. Hernández, C. J. C. Bennett, C. E. Junkermeier, S. D. Tsoi, F. J. Bezares, R. Stine, J. T. Robinson, E. H. Lock, D. R. Boris, B. D. Pate, J. D. Caldwell, T. L. Reinecke, P. E. Sheehan and S. G. Walton, Chemical Gradients on Graphene To Drive Droplet Motion, *ACS Nano*, 2013, **7**, 4746–4755, DOI: **10.1021/nn304267b**.

23  R. Garg, N. K. Dutta and N. R. Choudhury, Work Function Engineering of Graphene, *Nanomaterials*, 2014, **4**, 267–300, DOI: **10.3390/nano4020267**.

24  C. M. Mate, G. M. McClelland, R. Erlandsson and S. Chiang, Atomic-scale friction of a tungsten tip on a graphite surface, *Phys. Rev. Lett.*, 1987, **59**, 1942, DOI: **10.1007/978-94-011-1812-5_35**.

25  Y. Kuwahara, Muscovite surface structure imaged by fluid contact mode AFM, *Phys. Chem. Miner.*, 1999, **26**, 198–205, DOI: **10.1007/s002690050177**.

26  S. Decossas, L. Patrone, A. M. Bonnot, F. Comin, M. Derivaz, A. Barski and J. Chevrier, Nanomanipulation by atomic force microscopy of carbon nanotubes on a nanostructured surface, *Surf. Sci.*, 2003, **543**, 57–62, DOI: **10.1016/S0039-6028(03)00919-1**.

27  P. Ares, M. Pisarra, P. Segovia, C. Díaz, F. Martín, E. G. Michel, F. Zamora, C. Gómez-Navarro and J. Gómez-Herrero, Tunable Graphene Electronics with Local Ultrahigh Pressure, *Adv. Funct. Mater.*, 2019, **29**(8), 1806715, DOI: **10.1002/adfm.201806715**.

28  B. P. Epps and E. M. Krivitzky, Singular value decomposition of noisy data: noise filtering, *Exp. Fluids*, 2019, **60**, 126, DOI: **10.1007/s00348-019-2768-4**.

29  O. Alter and G. H. Golub, Singular Value Decomposition of Genome-Scale mRNA Lengths Distribution Reveals Asymmetry in RNA Gel Electrophoresis Band Broadening, *Proc. Natl. Acad. Sci. U. S. A.*, 2006, **103**(32), 11828–11833, DOI: **10.1073/pnas.0604756103**.

30  D. C. Elias, R. R. Nair, T. M. G. Mohiuddin, S. V. Morozov, P. Blake, M. P. Halsall, A. C. Ferrari, D. W. Boukhvalov, M. I. Katsnelson, A. K. Geim and K. S. Novoselov, Control of Graphene's Properties by Reversible Hydrogenation: Evidence for Graphane, *Science*, 2009, **323**(5914), 610–613, DOI: **https://www.science.org/doi/10.1126/science.1167130**.

31  S. D. Sherpa, S. A. Paniagua, G. Levitin, S. R. Marder, M. D. Williams and D. W. Hess, Photoelectron spectroscopy studies of plasma-fluorinated epitaxial graphene, *J. Vac. Sci. Technol., B: Nanotechnol. Microelectron.: Mater., Process., Meas., Phenom.*, 2012, **30**, 03D102, DOI: **10.1116/1.3688760**.

32  R. J. W. E. Lahaye, H. K. Jeong, C. Y. Park and Y. H. Lee, Density functional theory study of graphite oxide for different oxidation levels, *Phys. Rev. B*, 2009, **79**, 125435, DOI: **10.1103/PhysRevB.79.125435**.

33  K. Kim, Z. Lee, W. Regan, C. Kisielowski, M. F. Crommie and A. Zettl, Grain Boundary Mapping in Polycrystalline Graphene, *ACS Nano*, 2011, **5**(3), 2142–2146, DOI: **10.1021/nn1033423**.

34  L. Lin, J. Zhang, H. Su, J. Li, L. Sun, Z. Wang, F. Xu, C. Liu, S. Lopatin, Y. Zhu, K. Jia, S. Chen, D. Rui, J. Sun, R. Xue, P. Gao, N. Kang, Y. Han, H. Q. Xu, Y. Cao, K. S. Novoselov, Z. Tian, B. Ren, H. Peng and Z. Liu, Towards super-clean graphene, *Nat. Commun.*, 2019, **10**, 1912, DOI: **10.1038/s41467-019-09565-4**.

35  C. Sun, S.-J. Ko, S. Jung, C. Wang, D. Lee, J.-G. Kim and Y. Kim, Visualization of electrochemical behavior in carbon steel assisted by machine learning, *Appl. Surf. Sci.*, 2021, **563**, 150412, DOI: **10.1016/j.apsusc.2021.150412**.

36  D. Xu and Y. Tian, A Comprehensive Survey of Clustering Algorithms, *Ann. Data Sci.*, 2015, **2**, 165–193, DOI: **10.1007/s40745-015-0040-1**.